Exploring Recombination Dynamics and Photocurrent Dependance in Methylammonium Lead Halide Perovskite Nanostructures

Eliovardo Gonzalez, Rui Xiao, Yasen Hou, Dong Yu

[1]Department of Physics, California State University San Bernardino, 5500 University Pwky, San Bernardino, California 92407, United States

[2]Department of Physics, University of California, One Shields Ave, Davis, California 95616, United States

Keywords: perovskite, nanostructures, photocurrent, scanning photocurrent microscopy, photonics

Abstract: We investigate solution-growth and photovoltaic properties of single-crystal methylammonium lead iodide ($MAPbI_3$) nanostructures with scanning photocurrent microscopy (SPCM) and kelvin probe force microscopy (KPFM). Perovskite nanostructures are synthesized in a solution reaction between lead iodide (PbI_2) and methylammonium iodide (MAI) via dissolution and recrystallization mechanisms yielding 15-30um long nanostructures with varying widths. Perovskite samples are fabricated with Schottky contacts to pre-patterned gold electrodes displaying sensitive photocurrent under illumination. Minority carrier diffusion length is determined to be between 10-20um via SPCM measurements, significantly longer than previously reported results for polycrystalline thin films. Photocurrent is significantly stronger when laser is scanned on the nanostructure edge, this can be understood by the enhancement of light coupling and longer optical path due to refraction at this location.

Introduction

Hybrid organic-inorganic metal halide perovskite compounds have recently displayed significant potential for photovoltaic solar cells. In five years of academic research power conversion efficiencies have increased from 3% to over 20%.[1-7] Perovskite is more cost-effective than established photovoltaic devices due to the solution growth mechanisms and lacks the need for expensive purification processes required for leading competitors such as Silicon. Charge transport and recombination dynamics remain unclear due to the previous focus on polycrystalline thin films, which can convolute the understanding of intrinsic properties because of grain boundaries where the photoluminescence is significantly weaker and exhibits faster nonradiative decay. [8] It has recently been reported that single crystals with lower impurity defects may result in more efficient solar power conversion.[9] The study of single-crystal perovskite nanostructures offers a better basis for understanding the intrinsic properties of such a material. Single crystal perovskite nanostructures greatly simplify the interpretation of experimental results. In this study we have synthesized single crystal methylammonium lead iodide ($MAPbI_3$) nanostructures utilizing a solution growth method[10].

Previously, most optoelectronic studies of metal halide perovskites have been performed under global illumination where the entire sample is subjected to uniform light intensity. Scanning photocurrent microscopy (SPCM) utilizes a continuous wave laser to extract important physical properties from one and two dimensional nanostructures including: internal electric field distribution, carrier diffusion length, band bending, and barrier heights[11-17]. This is accomplished by precisely focusing a laser beam and raster-scanning at the surface of a planar electronic device while light reflection and photocurrent are recorded as a function of laser position. The use of scanning photocurrent microscopy, a relatively new technique, has enabled

spatially resolved optoelectronic measurements giving insight to intrinsic properties not afforded by global illumination. The penetration depth of injected carriers can be controlled by varying the wavelength of incident light allowing insight into the photocurrent distribution along the vertical dimension of the device. By varying penetration depth we achieve a three dimensional photocurrent mapping technique to single crystal perovskite nanostructures allowing for further understanding of semiconductor band structure, charge carrier diffusion length, and photon transport/recombination dynamics in hybrid perovskite.

Device Fabrication

Methylammonium lead iodide ($MAPbI_3$) nanostructures are synthesized via solution reaction between lead iodide (PbI_2) and methylammonium iodide (MAI) through a dissolution and reaction mechanism. This is achieved by first depositing lead acetate ($PbAc_2$) - film on a glass slide by drop-casting an aqueous solution of $PbAc_2*3H_2O$ with a concentration of 90mg/mL. The film is then dried in oven with the temperature set to 60 degrees Celsius. The concentration of $PbAc_2$ to be deposited on the glass slide is roughly $2mg/cm^2$. After drying, the glass slide is placed film side down into a reacting vial filled with 1mL of 40mg/mL solution of MAI in isopropanol. The reacting vials are then placed in the oven, again at 60 degrees Celsius, for 72 hours. After 72 hours the reaction is complete and glass slides are removed from the MAI/isopropanol solution and stored. Storing in air is suitable although it should be noted that storing under nitrogen can extend lifetime and avoid oxidation [See Figure 1a]. The perovskite

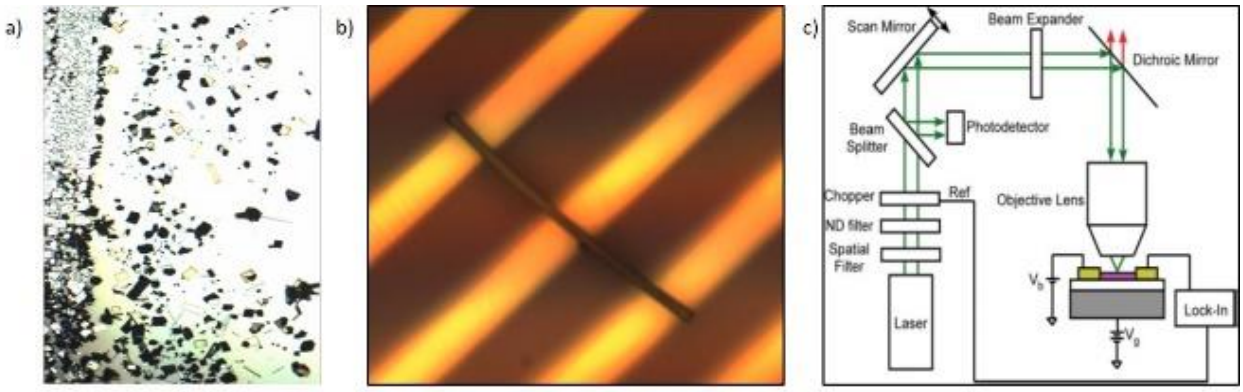

Figure 1: A) 10x zoom image samples immediately after growth reaction is complete. **B)** 100x zoom image of device after being transferred to pre-patterned electrodes. **C)** Experimental setup of scanning photocurrent microscopy (SPCM).

single crystals are then directly transferred to pre-patterned gold (Au) electrodes with contacts on both ends of the perovskite for optimal investigation of electronic properties [See Figure 1b]. The pre-patterned electrodes are prepared using electron beam lithography.

Optoelectronic Measurement Technique

Perovskite nanostructure devices were investigated using scanning photocurrent microscopy (SPCM) to understand diffusion length, internal electric field distribution, and photocurrent mapping. Additionally, kelvin probe force microscopy (KPFM) was used to gain insight to the contact barrier profiles and surface potential distribution. Experimental setup of SPCM is composed of four main components: an excitation source, position controller, focusing optics, and an electrical measurement unit [see Figure 1c]. Light is first generated by a continuous wave laser and directed through a series of optical filters. It is first passed through a spatial filter to remove higher-order spatial modes and provide a Gaussian laser profile to pass through subsequent optics. The next filter is a neutral density filter which allows for control of laser intensity. The optical chopper modulates the light source allowing electrical noise of photocurrent signal to be reduced. The resulting light is then directed through a beam splitter towards an X-Y scan mirror. The X-Y scan mirror is electronically controlled and is what allows for the raster-scanning of laser beam profile. Light then passes through a beam expander and into

a microscope with a high numerical aperture objective lens where it is focused into a diffraction limited spot on the sample below. The photocurrent is then recorded by a lock-in amplifier. Addition of a photodetector also allows for reflection data to be obtained. SPCM measurements will yield both spatially resolved photocurrent and reflection data in a 2-D image. KPFM measurements allow for insight to contact barrier profiles by measuring the potential difference between materials as a function of distance. KPFM measurements were performed in an atomic force microscope where the cantilever tip does not come into contact with the sample. This allows for insight into material work functions at the atomic and molecular scale. The work function relates to many surface phenomena including: band bending in semiconductors, doping profile, and charge trapping.

Results and Discussion

Prepared perovskite devices are conductive under illumination, however, very insulating in darkness. Photoconductance of these nanostructures was tested by illuminating the device with a diffraction limited laser spot of varying intensity, the laser was focused on the center and edge of the sample. Under illumination, the current-voltage (I-V_{sd}) curves are non-linear and current reaches saturation when the magnitude of the source-drain voltage (V_{sd}) is above a certain threshold voltage (V_{th}) which implies energy barriers at both contacts [Figure 2a]. These non-linear I-V_{sd} curves can be understood by modeling the device as two back-to-back diodes which

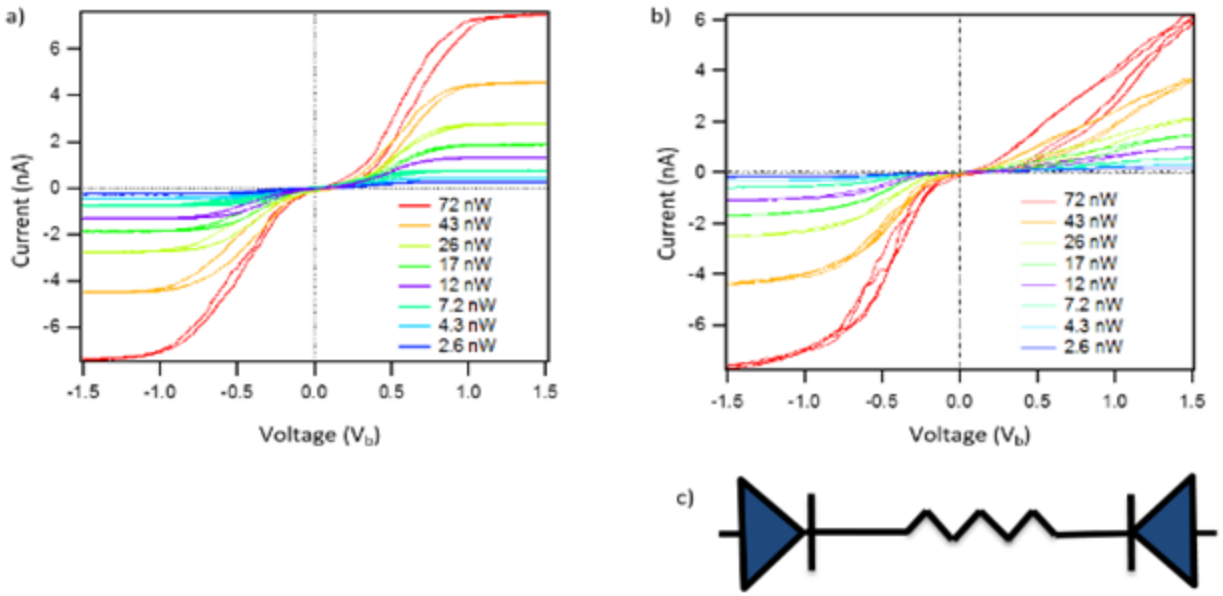

Figure 2: A) I-V_b curve with laser positioned at center. Current saturates for both positive and negative polarities. **B)** I-V_b curve with laser at pre-amp electrode. Current does not saturate for reverse biased electrode. **C)** Back-to-back diode contact model.

represent the contact barriers [Figure 1c]. At relatively high V_{sd} one diode will be reverse biased and the other forward biased with the reverse biased diode limiting the current. Current in the saturation region also increases linearly with light intensity [Figure 1b]. Upon examination of I-V_{sd} characteristics at low source-drain voltage we noted a few interesting observations: (1) I-V_{sd} curves demonstrate hysteretic behavior; (2) current increases linearly with V_{sd}; (3) current fluctuates prior to reaching saturation. The hysteretic behavior has been observed upon forward and backward bias voltage scans.

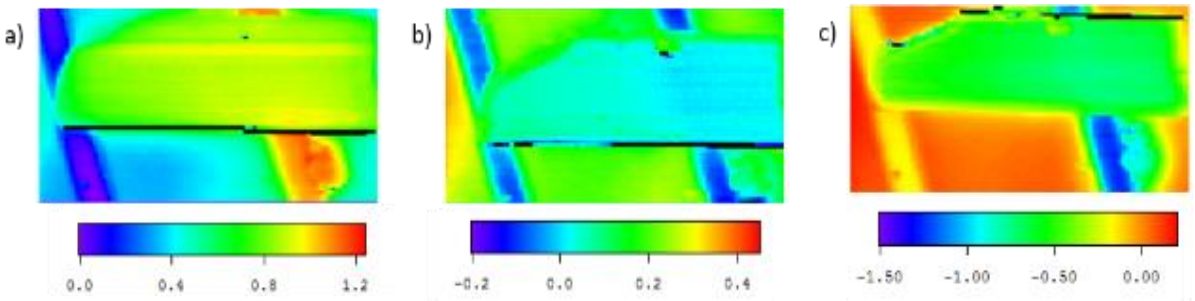

Figure 3: Legend indicates potential in volts **A)** KPFM at positive 2V bias, largest potential difference at reversely biased contact. **B)** KPFM at zero bias, potential difference same at both contacts. **C)** KPFM at negative 2V bias.

To confirm the back-to-back diode model for the contact barriers a surface potential mapping of the device was performed using Kelvin probe force microscopy (KPFM). The surface potential distribution is non-uniform at 2V, 0V, and -2V [Figure 3a, 3b, 3c, respectively]**.** The potential drop is large at the electrode contacts (>1V) and small along the nanostructure (<0.2V). Depending on the polarity of V_{sd}, the potential drop at the contact will be larger on one of the two electrodes. As the polarity flips, so does potential drop on the electrodes. This confirms the back-to-back diode model since the large potential drop will always be on the reverse biased electrode. In addition to the back-to-back diode model this data also confirms a Schottky junction at the perovskite and gold interface.

Wavelength dependence of photocurrent was also conducted via SPCM. At short wavelengths (<770nm) photocurrent distribution is relatively uniform as the laser is scanned on the surface of the nanostructure. Interestingly, at longer wavelengths (>780nm) the photocurrent distribution becomes non-uniform with enhancement at the edge and electrodes [Figure 4 a-f]. The enhancement at the electrodes can be understood in terms of the absorption length of light; at shorter wavelengths absorption is mostly occurring near the sample surface whereas longer wavelengths can penetrate deeper into the material. Longer wavelengths can then be reflected by the gold electrodes increasing absorption and, consequently, photocurrent. The photocurrent enhancement at the edges is understood in terms of refraction. When the laser is focused in the center light travels predominantly in a vertical direction after refraction at the surface. When the laser is refracted at the edge of the nanostructure the light travels through a more horizontal

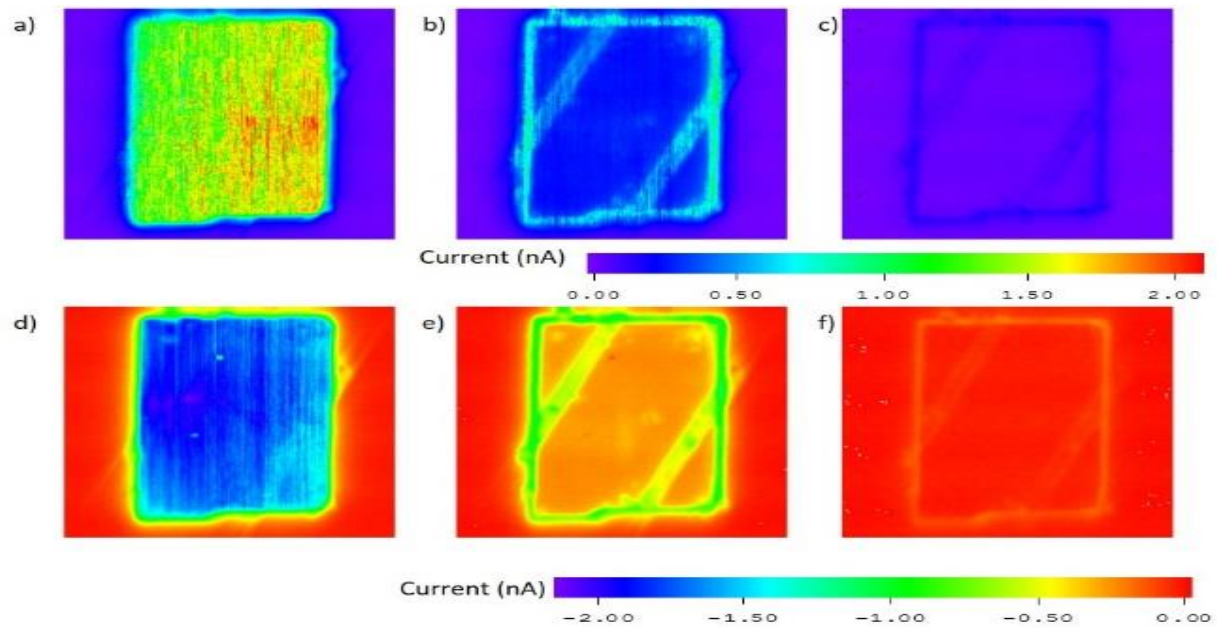

Figure 4: A-C) Positive bias scan. **D-F)** Negative Bias scan. All images in order of increasing wavelength from left to right (600nm, 770nm, 800nm).

optical path increasing the amount of light absorbed.. This enhancement of photocurrent can be exploited to increase absorption and solar power energy conversion during fabrication. Diffusion length has been determined to be ~10-17um via SPCM measurements. At lower laser intensity

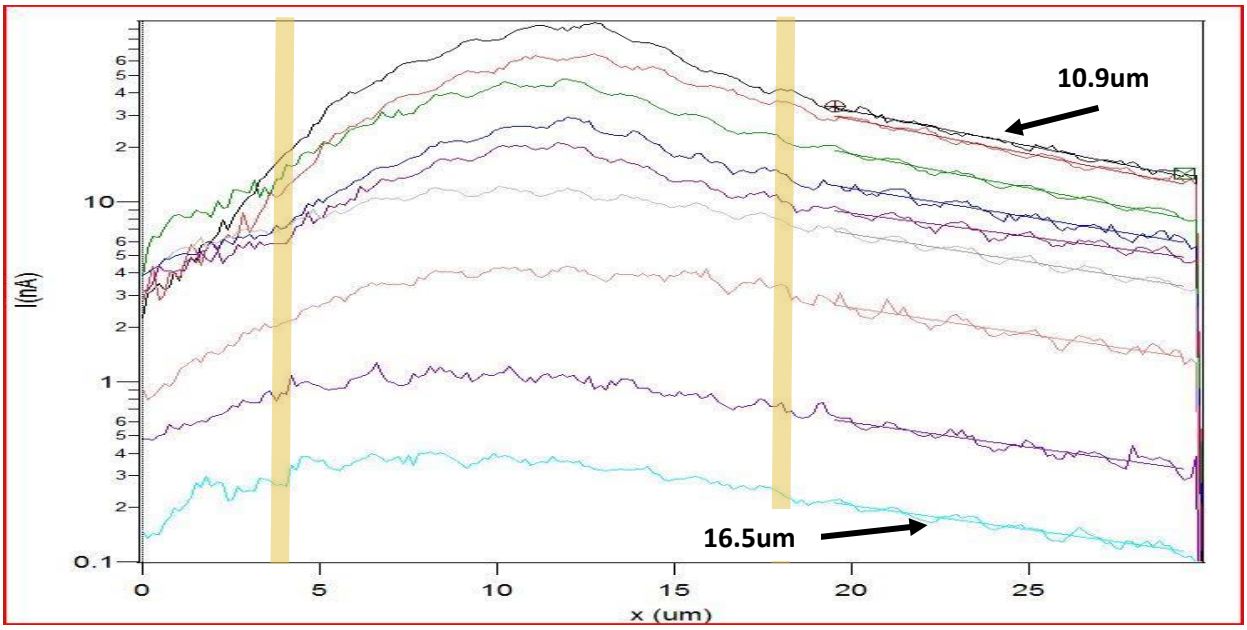

Figure 5: Current vs. Position (log scale). Electrodes modeled by gold vertical lines, diffusion length (black arrows) measured outside of the uniform electric field between them.

diffusion length is inversely proportional to carrier density. It must be noted diffusion length is dependent on carrier mobility and lifetime, at higher laser intensity the carrier density is increased and diffusion length is decreased. In conclusion, photocurrent is enhanced at longer wavelengths, I-V curves and KPFM measurements confirm back-to-back diode model, photocurrent increases proportionally with V_b, diffusion length determined to be ~10-17um and increases at lower laser intensity [Figure 5]. Future research could include exploiting the geometry of perovskite to increase solar power conversion efficiencies.

References

(1) Lee, M. M.; Teuscher, J.; Miyasaka, T.; Murakami, T. N.; Snaith, H. J. *Science* **2012,** *338*, 643-647.
(2) Heo, J. H.; Im, S. H.; Noh, J. H.; Mandal, T. N.; Lim, C. S.; Chang, J. A.; Lee, Y. H.; Kim, H. J.; Sarkar, A.; Nazeeruddin, M. K.; Gratzel, M.; Seok, S. I. *Nat. Photonics* **2013,** *7*, 487-492.
(3) Liu, M. Z.; Johnston, M. B.; Snaith, H. J. *Nature* **2013,** *501*, 395-398.
(4) Mei, A. Y.; Li, X.; Liu, L. F.; Ku, Z. L.; Liu, T. F.; Rong, Y. G.; Xu, M.; Hu, M.; Chen, J. Z.; Yang, Y.; Gratzel, M.; Han, H. W. *Science* **2014,** *345*, 295-298.
(5) Burschka, J.; Pellet, N.; Moon, S. J.; Humphry-Baker, R.; Gao, P.; Nazeeruddin, M. K.; Gratzel, M. *Nature* **2013,** *499*, 316-319.
(6) Zhou, H. P.; Chen, Q.; Li, G.; Luo, S.; Song, T. B.; Duan, H. S.; Hong, Z. R.; You, J. B.; Liu, Y. S.; Yang, Y. *Science* **2014,** *345*, 542-546.
(7) Jeon, N. J.; Noh, J. H.; Yang, W. S.; Kim, Y. C.; Ryu, S.; Seo, J.; Seok, S. I. *Nature* **2015,** *517*, 476 480.
(8) de Quilettes, D. W.; Vorpahl, S. M.; Stranks, S. D.; Nagaoka, H.; Eperon, G. E.; Ziffer, M. E.; Snaith, H. J.; Ginger, D. S. *Science* **2015,** *348*, 683-686.
(9) Im, J.-H.; Luo, J.; Franckevičius, M.; Pellet, N.; Gao, P.; Moehl, T.; Zakeeruddin, S. M.; Nazeeruddin, M. K.; Grätzel, M.; Park, N.-G. *Nano Lett.* **2015,** *15*, 2120-2126.
(10) Fu, Y.; Meng, F.; Rowley, M. B.; Thompson, B. J.; Shearer, M. J.; Ma, D.; Hamers, R. J.; Wright, J. C.; Jin, S. *J. Am. Chem. Soc.* **2015,** *137*, 5810-5818.
(11)Ahn, Y.; Dunning, J.; Park, J. *Nano Lett.* **2005,** *5*, 1367-1370.
(12)Gu, Y.; Romankiewicz, J. P.; David, J. K.; Lensch, J. L.; Lauhon, L. J. *Nano Lett.* **2006,** *6*, 948-952.
(13)Ahn, Y. H.; Tsen, A. W.; Kim, B.; Park, Y. W.; Park, J. *Nano Lett.* **2007,** *7*, 3320-3323.
(14)Doh, Y.-J.; Maher, K. N.; Ouyang, L.; Yu, C. L.; Park, H.; Park, J. *Nano Lett.* **2008,** *8*, 4552-4556.
(15)Allen, J. E.; Hemesath, E. R.; Lauhon, L. J. *Nano Lett.* **2009,** *9*, 1903-1908.
(16)Graham, R.; Miller, C.; Oh, E.; Yu, D. *Nano Lett.* **2011,** *11*, 717-722.
(17)Putnam, M. C.; Turner-Evans, D. B.; Kelzenberg, M. D.; Boettcher, S. W.; Lewis, N. S.; Atwater, H. A. *Appl. Phys. Lett.* **2009,** *95*, 163116-3.